molecules

MDPI

Article

Erucic Acid-Rich Yellow Mustard Oil Improves Insulin Resistance in KK-A^y Mice

Asako Takahashi [1], Mayu Ishizaki [1], Yoshifumi Kimira [2], Yukari Egashira [1] and Shizuka Hirai [1,*]

[1] Laboratory of Food Nutrition, Division of Applied Biochemistry, Graduate School of Horticulture, Chiba University, 648, Matsudo, Matsudo-shi, Chiba 271-8510, Japan; acaa1227@chiba-u.jp (A.T.); afga8471@chiba-u.jp (M.I.); egashira@faculty.chiba-u.jp (Y.E.)

[2] Faculty of Pharmacy and Pharmaceutical Sciences, Josai University, 1-1 Keyakidai, Sakado-shi, Saitama 350-0295, Japan; kimira@josai.ac.jp

* Correspondence: shizuka@faculty.chiba-u.jp; Tel./Fax: +81-47-308-8859

Abstract: Obesity is a major risk factor for some metabolic disorders including type 2 diabetes. Enhancement of peroxisome proliferator-activated receptor (PPAR) γ, a master regulator of adipocyte differentiation, is known to increase insulin-sensitive small adipocytes. In contrast, decreased PPARγ activity is also reported to improve insulin resistance. We have previously identified erucic acid as a novel natural component suppressing PPARγ transcriptional activity. In this study, we investigated the effect of erucic acid-rich yellow mustard oil (YMO) on obese/diabetic KK-A^y mice. An in vitro luciferase reporter assay and mesenchymal stem cell (MSC) differentiation assay revealed that 25 μg/mL YMO significantly inhibited PPARγ transcriptional activity and differentiation of MSCs into adipocytes but promoted their differentiation into osteoblasts. In KK-A^y mice, dietary intake of 7.0% (*w*/*w*) YMO significantly decreased the surrogate indexes for insulin resistance and the infiltration of macrophages into adipose tissue. Furthermore, 7.0% YMO increased bone mineral density. These results suggest that YMO can ameliorate obesity-induced metabolic disorders.

Keywords: yellow mustard oil; erucic acid; obesity; type 2 diabetes; insulin resistance; inflammation

Citation: Takahashi, A.; Ishizaki, M.; Kimira, Y.; Egashira, Y.; Hirai, S. Erucic Acid-Rich Yellow Mustard Oil Improves Insulin Resistance in KK-A^y Mice. *Molecules* **2021**, *26*, 546. https://doi.org/10.3390/molecules26030546

Academic Editor: Lars Porskjær Christensen

Received: 9 December 2020

Accepted: 16 January 2021

Published: 21 January 2021

1. Introduction

Obesity is a major risk factor for atherosclerosis, insulin resistance, type 2 diabetes, cardiovascular disease, hypertension, and dyslipidemia, called metabolic syndrome [1]. Obesity is considered to be the result of an increase in the number and size of adipocytes [2]. Peroxisome proliferator-activated receptor (PPAR) γ, the master regulator of adipocyte differentiation, is a ligand-responsive transcription factor. Synthetic PPARγ agonists such as thiazolidinediones are used as antidiabetic agents because they strongly promote adipocyte differentiation and increases insulin-sensitive, small adipocytes [3,4]. However, such PPARγ agonists are associated with some side effects, including body weight gain [5] and bone loss [6,7]. On the other hand, it has been reported that high-fat diet (HFD)-induced adipocyte hypertrophy and insulin resistance are improved in heterozygous PPARγ-deficient mice as compared with the wild type mice [8–10]. Synthetic PPARγ antagonists, GW9662 and bisphenol A diglycidyl ether, have also been reported to improve insulin resistance and obesity [11,12]. Furthermore, these PPARγ antagonists increase bone mass and osteoblast differentiation from mesenchymal stem cells (MSCs) [13,14]. Therefore, moderately decreased PPARγ activity is expected to improve insulin resistance and increase bone mass without inducing obesity.

In our previous study, we found that erucic acid isolated from rosemary promotes the differentiation of MSCs into osteoblasts but inhibits the differentiation into adipocytes by suppressing PPARγ transcriptional activity [15]. Erucic acid is one of the monounsaturated fatty acids widely found in Brassicaceae plants such as rapeseed and mustard [16,17]. In particular, mustard oil is rich in erucic acid [18]. However, there are few reports on the biological function of erucic acid.

In the present study, we investigated the effect of yellow mustard oil (YMO), which contains a large amount of erucic acid (approximately 37.0% in fatty acids), on metabolic disorders in obese/diabetic KK-A^y mice. We revealed that 25 μg/mL YMO significantly decreased PPARγ transcriptional activity and inhibited MSCs differentiation into adipocytes but enhanced their differentiation into osteoblasts. In KK-A^y mice, 7.0% YMO intake decreased surrogate indexes for insulin resistance and improved inflammation in adipose tissue. Furthermore, 7.0% YMO increased bone mineral density. These findings indicate that YMO may have beneficial effects on improving glucose and bone metabolism disorders induced by obesity and diabetes.

2. Results

2.1. YMO Suppressed PPARγ Transcriptional Activity and Differentiation of MSCs into Adipocytes

Since most fatty acids in vegetable oils are bound to triglyceride [19], we used the YMO hydrolyzed to free fatty acids in in vitro experiments. When we examined the effect of hydrolyzed YMO on PPARγ transcriptional activity by luciferase reporter assay, 25 μg/mL YMO and 5 μM GW9662 significantly decreased troglitazone-induced PPARγ transcriptional activity (Figure 1A). YMO used in this study contained 36.97% erucic acid (Figure 2, Table 1). The hydrolyzed YMO also showed a similar fatty acid composition (Supplementary Table S1). Therefore, YMO that showed significant decrease of PPARγ transcriptional activity contained about 27.24 μM erucic acid, which is comparable to the erucic acid concentration (25 μM) that suppressed PPARγ activity in our previous study [15]. Inhibitors of PPARγ transcriptional activity have been reported to regulate MSCs differentiation [14]. In the present study, 15–40 μg/mL YMO significantly decreased the number of Oil Red O$^+$ adipocytes (Figure 1B) and increased that of alkaline phosphatase (ALP) $^+$ osteoblasts (Figure 1C).

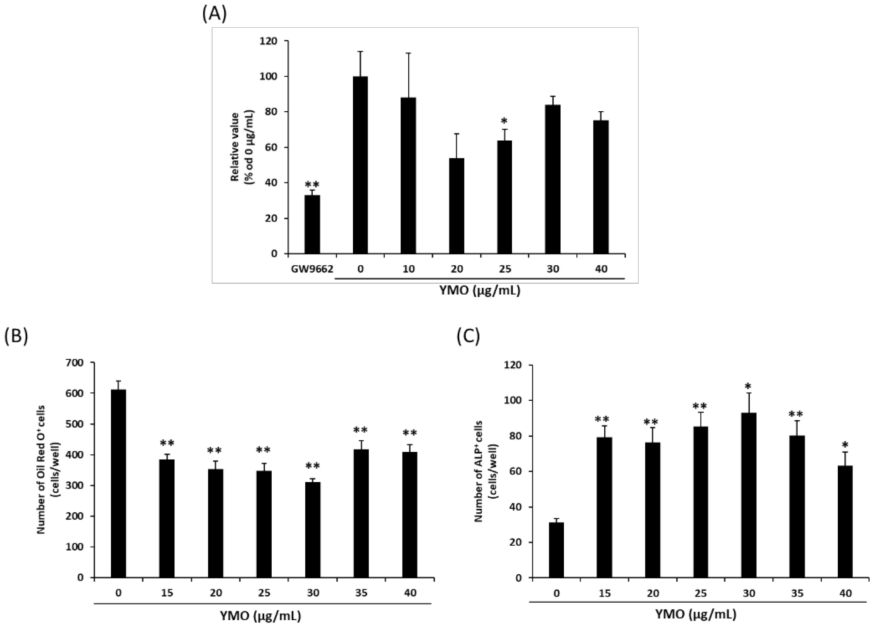

Figure 1. Effect of YMO on peroxisome proliferator activated receptor γ (PPARγ) transcriptional activity and differentiation of C3H10T1/2 cells. (**A**) Effect of 0–40 μg/mL YMO on PPARγ transcriptional activity in the presence of 5 μM troglitazone. Relative luciferase activities were expressed as percentage of vehicle control. (**B**,**C**) Effect of 0–40 μg/mL YMO treatment for 14 days on differentiation of C3H10T1/2 cells. A number of Oil Red O$^+$ cells (**B**) and of ALP$^+$ cells (**C**) in each well were counted under light microscope. Values are mean ± SE, n = 4–5. ** $p < 0.01$, * $p < 0.05$ versus 0 μg/mL.

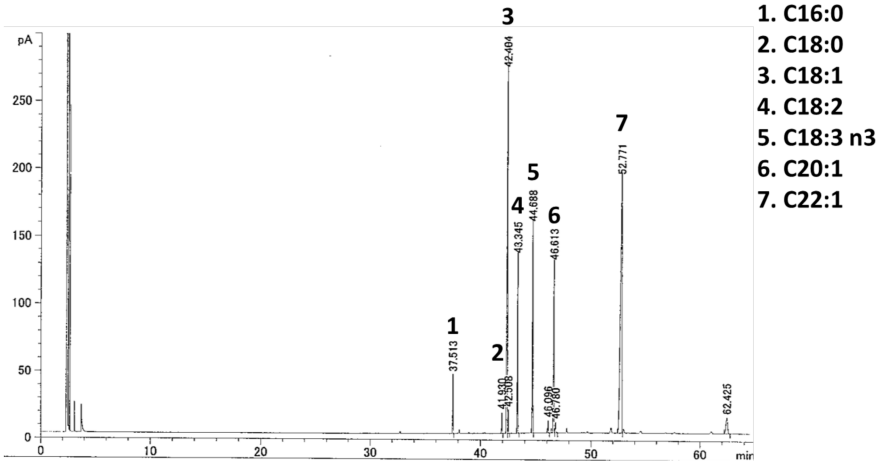

Figure 2. Gas chromatograph with flame ionization detector (GC-FID) chromatogram of YMO.

Table 1. Composition of fatty acids in YMO.

Fatty Acid (%)	YMO
C16:0	2.61
C18:0	1.05
C18:1	24.35
C18:2	8.92
C18:3 n3	10.49
C20:1	10.88
C22:1	36.97
Others	4.73

To reveal the molecular mechanism of which YMO suppressed adipocyte differentiation and enhanced osteoblast differentiation from MSCs, we measured the expression of adipocyte and osteoblast differentiation-related genes by real time PCR. Twenty-five μg/mL YMO significantly decreased mRNA expression of PPARγ at day 12 and 14 (Figure 3A). The expression of PPARγ target genes, aP2 and LPL, were suppressed by YMO earlier than the decrease in PPARγ mRNA expression (Figure 3B,C). On the other hand, mRNA expression of osteoblast differentiation markers, ALP and Col1, were increased by YMO at days 12 and 14 (Figure 3F) and at days 8 and 12 (Figure 3G), respectively. The expression of Runx2 and Osterix, which are known as transcription factors involved in the induction of ALP and Col1 expression [20,21], were largely unaffected by YMO (Figure 3D,E).

2.2. YMO Suppressed Fat Accumulation in KK-A^y Mice

PPARγ antagonists have been reported to suppress HFD diet-induced obesity [11,12]. Therefore, we examined the effect of YMO on fat accumulation in KK-A^y mice. As a result, 3.5% YMO intake significantly reduced body weight and subcutaneous adipose tissue weight (Table 2). On the other hand, perirenal adipose tissue weight was significantly reduced in 7.0% YMO group (Table 2), which was accompanied by decreased mRNA expression of PPARγ target genes, *aP2* and *LPL* (Figure 4). However, GW9662 did not affect either body weight, adipose tissue weight, or expression of adipocyte differentiation marker genes (Table 2, Figure 4)

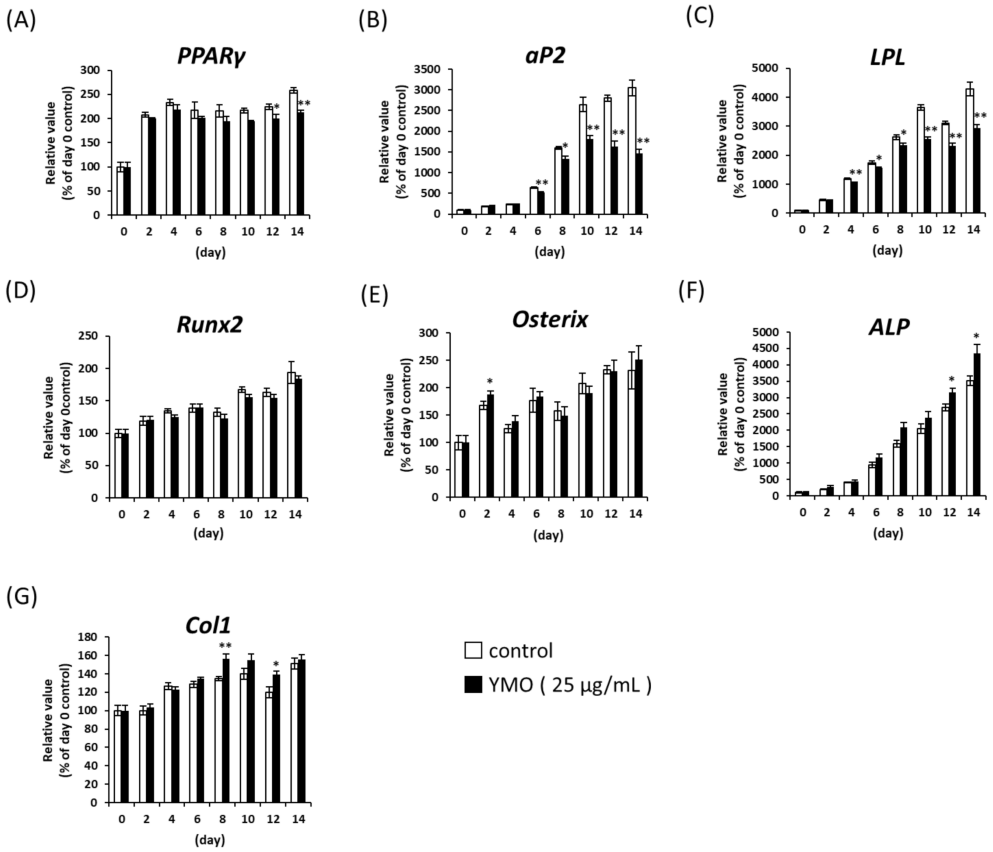

Figure 3. Effect of YMO on the expression of adipocyte or osteoblast marker genes. C3H10T1/2 cells were differentiated and treated with ethanol or YMO (25 μg/mL) for 14 days. mRNA expression levels of adipocyte marker genes (**A**–**C**) and osteoblast marker genes (**D**–**G**) were measured by real-time PCR. Relative mRNA expressions were expressed as percentage of day 0 control. Values are mean ± SE, n = 4–5. ** $p < 0.01$, * $p < 0.05$ versus each day control.

Table 2. Effect of YMO on final body weight and white adipose tissue weight in KK-A^y mice.

	Control	GW9662	1.0% YMO	3.5% YMO	7.0% YMO
Final body weight (g)	42.29 ± 0.70	40.16 ± 0.95	41.98 ± 1.36	39.59 ± 0.68 *	41.41 ± 0.84
Subcutaneous adipose tissue (g)	1.62 ± 0.08	1.41 ± 0.05	1.63 ± 0.10	1.21 ± 0.10 *	1.47 ± 0.07
Perirenal adipose tissue (g)	0.91 ± 0.09	0.94 ± 0.07	0.88 ± 0.10	0.66 ± 0.06	0.59 ± 0.08 *
Mesenteric adipose tissue (g)	1.09 ± 0.04	0.99 ± 0.05	1.21 ± 0.03	0.96 ± 0.06	1.12 ± 0.05
Epididymal adipose tissue (g)	1.04 ± 0.04	0.98 ± 0.03	1.03 ± 0.03	0.96 ± 0.04	1.05 ± 0.06

Values are mean ± SE, n = 10–11. * $p < 0.05$ versus control.

2.3. YMO Improved Insulin Resistance in KK-A^y Mice

To examine the effect of YMO on obesity-related development of insulin-resistance, we performed oral glucose tolerance test (OGTT). GW9662 significantly decreased plasma glucose and insulin levels compared to the control group (Figure 5A–D), leading to the significant decrease of homeostasis model assessment-insulin resistance (HOMA-IR) (Figure 5E) and increase of quantitative insulin-sensitivity check index (QUICKI) (Figure 5F) values, which are the surrogate indexes for insulin resistance. Although YMO did not significantly affect the area under the curve (AUC) of plasma glucose level (Figure 5B), AUC of plasma insulin level in 3.5% and 7.0% YMO groups was significantly decreased compared to the control group (Figure 5D). HOMA-IR value in 7.0% YMO group and QUICKI value in 3.5% and 7.0% YMO group were also significantly decreased (Figure 5E) and increased (Figure 5F), respectively, compared to the control group.

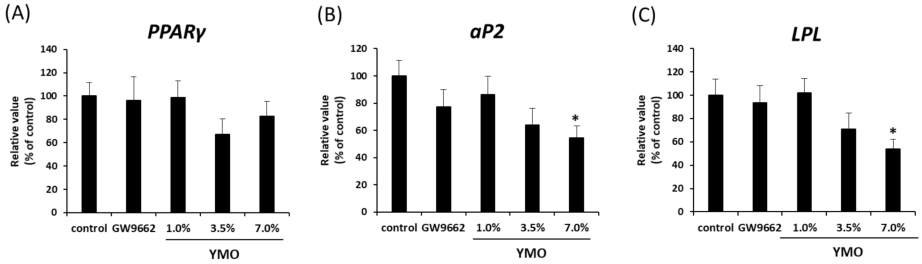

Figure 4. Effect of YMO on the expression of adipocyte differentiation marker genes in perirenal adipose tissue in KK-A^y mice. Perirenal adipose tissue was collected from KK-A^y mice fed with 1.0, 3.5, or 7.0% YMO for 16 weeks. mRNA expression levels of *PPARγ* (**A**), *aP2* (**B**), and *LPL* (**C**) were measured by real-time PCR. Relative mRNA expressions were expressed as percentage of control. Values are mean ± SE, n = 10–11. * $p < 0.05$ versus control.

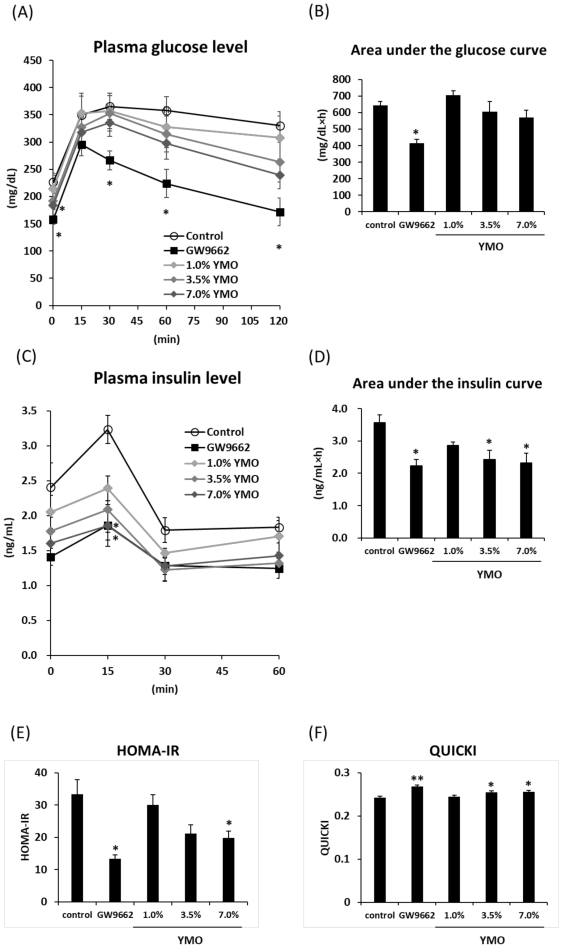

Figure 5. Effect of YMO on plasma glucose and insulin levels during oral glucose tolerance test (OGTT) in KK-A^y mice. OGTT was performed at 15 week of animal experiment. Plasma glucose level (**A**), area under the glucose curve (**B**), plasma insulin level (**C**), area under the insulin curve (**D**), homeostasis model assessment-insulin resistance (HOMA-IR) (**E**), quantitative insulin-sensitivity check index (QUICKI) (**F**) were measured in KK-A^y mice fed with 1.0, 3.5, or 7.0% YMO. Values are mean ± SE, n = 7–10 (**A**,**B**) and n = 5–7 (**C**–**F**). ** $p < 0.01$, * $p < 0.05$ versus control.

2.4. YMO Suppressed Infiltration of Macrophages into Adipose Tissue in KK-A^y Mice

We next investigated the morphological changes of perirenal adipose tissue in KK-A^y mice. Although YMO and GW9662 did not affect adipocyte size and number (Figure S1), 7.0% YMO and GW9662 significantly decreased crown-like structures (CLS) (Figure 6A,B) and

F4/80$^+$ (Figure 6A,C) areas. Furthermore, 3.5% and 7.0% YMO and GW9662 significantly decreased both the areas positive for a M1 macrophage marker, CD11c (Figure 6D), and a M2 macrophage marker, CD206 (Figure 6E). On the other hand, the ratio of CD206/CD11c area was significantly increased by 7.0% YMO and GW9662 groups (Figure 6F). Although mRNA expression levels of a macrophage marker, F4/80 (Figure 7A), and monocyte chemoattractant protein-1 (MCP-1) (Figure 7B), involved in macrophage infiltration, were not significantly different among the groups, mRNA expression of M1 macrophage markers, CD11c, Interleukin-1β (IL-1β), and tumor necrosis factor-α (TNF-α) (Figure 7C–E), and a M2 macrophage marker, CD206 (Figure 7F), in perirenal adipose tissue were significantly decreased in 3.5 and/or 7.0% YMO and GW9662 groups. Moreover, 7.0% YMO significantly decreased mRNA expression of another M2 macrophage marker, Ym1 (Figure 7G), but did not affect mRNA expression of arginase 1 (Arg1) (Figure 7H).

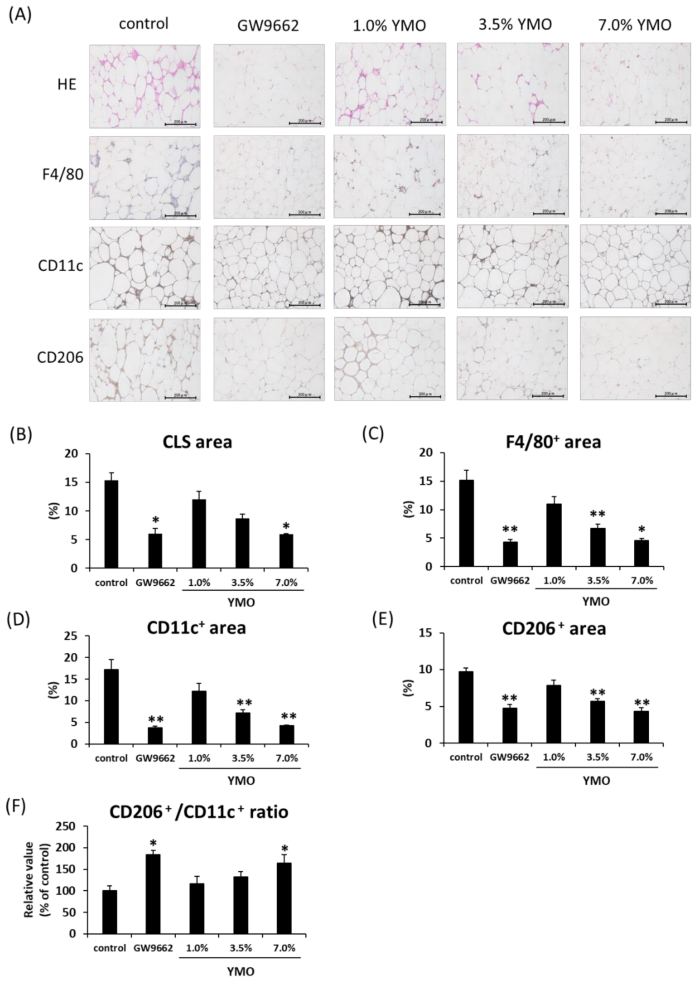

Figure 6. Effect of YMO on macrophage infiltration into perirenal adipose tissue in KK-A^y mice. Perirenal adipose tissue was collected from KK-A^y mice fed with 1.0, 3.5, or 7.0% YMO for 16 weeks. Paraffin sections of adipose tissue were stained with hematoxylin & eosin (HE), or immunostained with anti-F4/80, CD11c, or CD206 antibody. (**A**) Histological analytic image of HE staining and immunostainings, (**B**) Area of crown like structure (CLS), (**C**) F4/80$^+$ area, (**D**) CD11c$^+$ area, (**E**) CD206$^+$ area, (**F**) Ratio of CD206$^+$ area/CD11c$^+$ area. Values are mean ± SE, $n = 7$. ** $p < 0.01$, * $p < 0.05$ versus control.

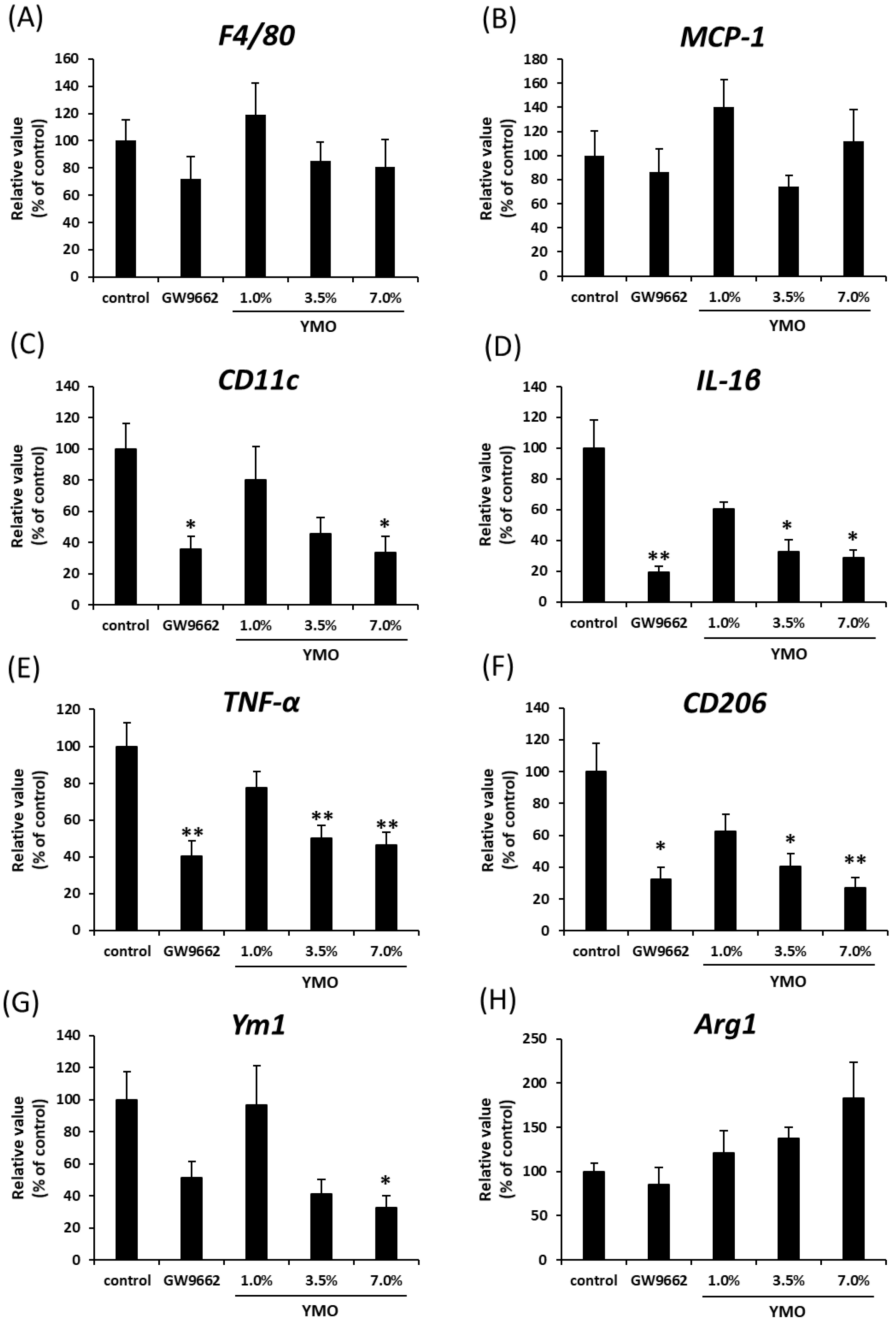

Figure 7. Effect of YMO on the expression of macrophage marker genes in perirenal adipose tissue in KK-A^y mice. mRNA expression levels of F4/80 (**A**), MCP-1 (**B**), M1 macrophage markers (**C**–**E**), and M2 macrophage markers (**F**–**H**) in perirenal adipose tissue were measured as described in Figure 3 legend. Values are mean ± SE, n = 10–11. ** $p < 0.01$, * $p < 0.05$ versus control.

2.5. YMO Increased Bone Mineral Density (BMD) and Osteoblastic Bone Formation Marker

It has been reported that bone mineral density (BMD) decreases in KK-A^y mice as the progression of obesity [22]. In the present study, total, cortical, and cancellous BMD in the right femur was significantly increased in 7.0% YMO group (Figure 8A–C). Similar result was observed in left femur (Supplementary Figure S2). Furthermore, plasma ALP activity, a marker of osteoblastic bone formation, was increased in 7.0% YMO group (Figure 8D), whereas plasma tartrate-resistant acid phosphatase (TRAP) activity, a marker of osteoclastic bone resorption, was not affected by YMO and GW9662 (Figure 8E).

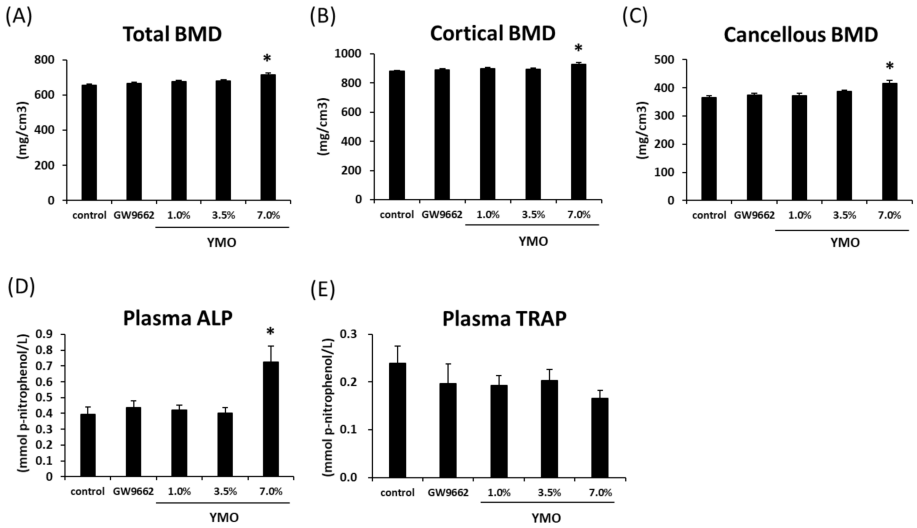

Figure 8. Effect of YMO on bone mineral density (BMD) and plasma bone metabolic markers in KK-A^y mice. Right femur was collected from KK-A^y mice fed with 1.0, 3.5, or 7.0% YMO for 16 weeks. Total BMD (**A**), cortical BMD (**B**), and cancellous BMD (**C**) were measured by peripheral quantitative computed tomography (pQCT). Plasma ALP (**D**) and TRAP (**E**) activities were measured as described in "Materials and Methods". Values are mean ± SE, n = 10–11. * $p < 0.05$ versus control.

3. Discussion

Adipose tissue plays an important role in the regulation of glucose metabolism throughout the body. It is reported that many kinds of synthetic [23,24] and natural [25,26] PPARγ agonists increase the number of insulin-sensitive small adipocytes by promoting adipocyte differentiation. On the other hand, it has been reported that heterozygous knock-out of PPARγ or moderate suppression of PPARγ activity also contribute to enhancement of insulin sensitivity without increasing adipocyte mass [8–10]. However, unlike PPARγ agonists, there are few natural components that have been reported to inhibit PPARγ transcriptional activity [27,28].

We previously identified erucic acid as a novel natural component with inhibitory effect of PPARγ transcriptional activity [15]. To evaluate the in vivo function of erucic acid, we used YMO, which is rich in erucic acid, in the present study. Twenty-five μg/mL YMO (corresponding to 27.24 μM erucic acid) significantly decreased PPARγ reporter activity and enhanced MSCs differentiation into osteoblasts rather than adipocytes. YMO dose-dependently decreased PPARγ reporter activity at a concentration of 20 or 25 μg/mL or less but restored the activity at concentration above 25 μg/mL. A similar result was shown with the effect of YMO on MSCs differentiation. YMO dose-dependently suppressed adipocyte differentiation and enhanced osteoblast differentiation at concentrations of 30 μg/mL or less, but the effect was attenuated at concentration above 30 μg/mL. In our previous study using erucic acid, the effects of erucic acid on decreasing PPARγ activity and regulating MSCs differentiation were also attenuated at concentrations above 25 μM [15], which may be due to changes in solubility with morphological changes of fatty acid depending on its concentration [29]. Further study will be needed to clarify the relationship between concentration-related morphological changes of erucic acid in YMO and its effect on PPARγ activity and differentiation of MSCs.

When we examined the in vivo effect of YMO in a KK-A^y obese/insulin-resistant model mice, YMO reduced perirenal adipose tissue weight and mRNA expression of PPARγ target genes but did not affect PPARγ mRNA expression. PPARγ agonists are known to increase the number of small adipocytes by promoting adipocyte differentiation [3,4], but YMO did not affect the average area and number of adipocytes. Furthermore, YMO also reduced the expression of PPARγ target genes earlier than the reduction of PPARγ mRNA expression in MSCs. These results suggest that YMO suppresses adipocyte

differentiation by reducing PPARγ activity rather than by reducing its mRNA expression. On the other hand, GW9662 showed no effect on body weight and adipose tissue weights. Previous report has shown that 0.1% GW9662 suppresses HFD-induced fat accumulation and weight gain in C57BL/6J mice [11]. Therefore, it was suggested that GW9662 concentration used in this study was insufficient to suppress fat accumulation in KK-A^y mice.

Obesity-induced insulin resistance is closely associated with macrophage infiltration into adipose tissue [30]. In obese animals, macrophages infiltrate into adipose tissues recruited by MCP-1 secreted from hypertrophied adipocytes [31]. Excess MCP-1 and inflammatory cytokines including TNF-α secreted from infiltrated macrophages, induce additional infiltration of macrophages and insulin resistance, respectively [32]. It is also known that the phenotype of macrophages in adipose tissue changes as the progression of obesity. M1 macrophages which increase with the progression of HFD-induced obesity highly express pro-inflammatory cytokines, including TNF-α, which is considered to be involved in insulin resistance [33]. On the other hand, M2 macrophages expressing anti-inflammatory cytokines are abundant in the adipose tissues in lean animals [34]. In this study, YMO and GW9662 improved HFD-induced insulin resistance. YMO and GW9662 decreased the area of CLS, an accumulation of immune cells surrounding adipocytes [35], and the positive area of F4/80, a macrophage marker expressed in both M1 and M2 [33] in perirenal adipose tissue. YMO and GW9662 reduced positive areas for both a M1 macrophage marker, CD11c, and a M2 macrophage marker, CD206. The mRNA expressions of M1 macrophage markers (*CD11c*, *IL-1β*, *TNF-α*) and M2 macrophage markers (*CD206*, *Ym1*) were also decreased by YMO and GW9662. However, M2/M1 ratio in adipose tissue was significantly increased by YMO and GW9662. These results suggest that YMO and GW9662 may increase insulin sensitivity by suppressing macrophage infiltration and increasing M2/M1 ratio in adipose tissue. Several reports have shown that the insulin-sensitizing effect of PPARγ ligands are exerted not by classical agonism but by inhibition of cyclin-dependent kinase (CDK) 5-mediated phosphorylation of PPARγ at Ser^{273} (pS273) [36–38]. PPARγ agonists are also known to exert anti-inflammatory effects through suppression of nuclear factor-kappa B (NF-κB) transcriptional activity without classical agonism [39]. Furthermore, PPARγ antagonist Gleevec is also suggested to ameliorate adipose tissue inflammation via inhibition of pS273 and NF-κB activation [40]. Therefore, YMO and GW9662 may suppress adipose tissue inflammation via similar mechanism. Further study is needed to clarify the detailed mechanism of anti-inflammation by YMO and GW9662.

In the present study, YMO promoted the differentiation of MSCs into osteoblasts, which was accompanied by increased mRNA expression of osteoblast differentiation markers, *ALP* and *Col1*, but not by the changes of mRNA expressions of *Runx2* and *Osterix*. Runx2 and Osterix are known as transcription factors involved in the induction of *ALP* and *Col1* expressions [20,21], but several studies have reported that *ALP* expression can be induced without changes of *Runx2* mRNA expression [41–45], which suggests the involvement of the binding activity of Runx2 to *ALP* promoter [41–43] or of other transcription factors [44,45]. In addition to obesity and diabetes, KK-A^y mice are reported to show a significantly lower BMD and blood level of bone formation markers compared to C57BL/6 normal mice, although they have no effect on blood bone resorption markers [22]. Therefore, we examined the effect of YMO on BMD and plasma bone metabolism markers in KK-A^y mice. In this study, 7.0% YMO significantly increased femoral BMD and plasma level of bone formation, indicated by ALP activity, without affecting the plasma level of bone resorption, indicated by TRAP. These results suggest that YMO may also suppress the decrease in BMD associated with diabetes by affecting osteoblast differentiation and/or its function. On the other hand, GW9662 did not affect BMD in KK-A^y mice. Beekman et al. [46] reported that administration of GW9662 did not affect bone loss in ovariectomized (OVX) mice. OVX-induced bone loss is a model of "high-turnover osteoporosis" often observed in postmenopausal women [47], caused by osteoclastic bone resorption greatly exceeding osteoblastic bone formation. On the other hand, the diabetic animal used in

this study is a model of "low-turnover osteoporosis" in which both bone formation and resorption are lower than normal, but even lower bone formation than resorption results in bone loss [48]. Therefore, components that activate osteoblastic bone formation may be effective in improving bone loss in diabetic models. To clarify the mechanism of increased BMD by YMO, it is necessary to examine the effect of higher concentration of GW9662 and/or the difference between GW9662 and YMO uptake into bone.

4. Materials and Methods

4.1. Chemicals

YMO was provided from Kewpie Corporation (Tokyo, Japan). A synthetic PPARγ agonist, troglitazone, and a synthetic PPARγ antagonist, GW9662, were purchased from FUJIFILM Wako Pure Chemical Corporation (Osaka, Japan). Ethanol and dimethyl sulfoxide (DMSO) were also obtained from FUJIFILM Wako Pure Chemical Corporation.

4.2. Hydrolyzation of YMO

For in vitro experiments, YMO was hydrolyzed to free fatty acids as follows; 100 mL of 1M KOH/ethanol solution was added to 10 g of silica gel-treated YMO and heated in a water bath at 80–100 °C for 30 min, and then 200 mL of water and 100 mL of diethyl ether were added and distributed. One hundred milliliter of diethyl ether and 100 mL of water were added to the aqueous layer and the ether layer, respectively, and further distributed. Approximately 6 mL of 4N HCl was added to the aqueous layer containing the saponified product, and then 100 mL of diethyl ether was added for further distribution. After removing water from the diethyl ether layer using sodium sulfate, a filtered and distilled sample was used for in vitro experiment.

4.3. Fatty Acid Analysis of YMO

Fifty milligrams of YMO or its hydrolyzed sample (each from Kewpie Corporation) and 5 mL of 0.5 mol/L sodium hydroxide-methanol solution were mixed and heated in a boiling water bath for 5–10 min. After adding 7 mL of boron trifluoride-methanol reagent (Sigma-Aldrich Co., St. Louis, MO, USA) and boiled for 2 min, 5 mL of hexane was added and heated for another 1 min. After adding about 140 mL of saturated saline, 1 mL of the hexane layer was transferred to a test tube and about 0.2 g of sodium sulfate was added to remove water, which was used as a sample solution for fatty acid analysis by gas chromatograph with flame ionization detector (GC-FID) (GC-6890N; Agilent Technologies Inc, Santa Clara, CA, USA) using an Omegawax® 250 Intuvo Capillary GC Column (L × I.D. 30 m × 0.25 mm, df 0.25 μm; Sigma-Aldrich, Supelco, PA, USA). The detected fatty acids were quantified with Supelco® 37 Component FAME Mix (Sigma-Aldrich, Supelco, PA, USA).

4.4. PPARγ Luciferase Reporter Assay

We performed a luciferase reporter assay according to our previous report [15]. Briefly, monkey CV-1 kidney cells (American Type Culture Collection, USA) reached 90% confluence on a 100-mm culture plate were transfected with a reporter vector (p4 × UASg-tk-Luc), an expression vector for a chimera protein for GAL4 DNA-binding domain and human PPARγ ligand-binding domain (pM-hPPARγ), and an internal control vector (pRL-CMV) for 4 h. These vectors were kindly provided by Prof. Teruo Kawada and Dr. Tsuyoshi Goto, Kyoto University. After transfection, cells were seeded at 5.00×10^3 cells/well on 96 well plates and treated with medium containing 5 μM troglitazone (FUJIFILM Wako) dissolved in DMSO and either each concentration (0, 10, 20, 25, 30, 40 μg/mL) of YMO dissolved in ethanol or 5 μM GW9662 (FUJIFILM Wako) dissolved in ethanol for 24 h. Luciferase reporter assay was performed using Dual-Glo luciferase assay system (Promega, Madison, WI, USA).

4.5. Culture of C3H10T1/2 Cells

Mouse C3H10T1/2 mesenchymal stem cells (JCRB Cell Bank, Osaka, Japan) were cultured in DMEM containing 10% FBS (Equitech-Bio Inc, Kerrville, TX, USA) and 100 U/mL penicillin and 100 μg/mL streptomycin (FUJIFILM Wako) at 37 °C under a humidified 5% CO_2 atmosphere. Cells were seeded at 1.25×10^5 cells/well on 24 well plates for staining or 2.50×10^5 cells/well on 12 well plates for RNA extraction. After reaching confluent, the culture medium was replaced with DMEM containing 10% FBS and 0, 15, 20, 25, 30, 35, or 40 μg/mL YMO dissolved in ethanol and changed every 2 days for 14 days.

4.6. Oil Red O and ALP Staining

Differentiated adipocytes and osteoblasts were evaluated by Oil Red O staining and ALP staining, respectively, according to the methods previously described [15]. Briefly, in Oil Red O staining, cells were stained with Oil Red O solution (0.5% Oil Red O/2-propanol diluted in water [3:2]) for 1 h. In ALP staining, cells were stained using Alkaline Phosphatase Staining kit (Cosmo Bio Co., LTD, Tokyo, Japan) according to the manufacturer's protocol. After staining, a grid seal (1806-009, AGC TECHNO GLASS Co., Ltd., Shizuoka, Japan) was attached to the bottom of the plate, and the number of Oil Red O^+ cells/well or that of ALP^+ cells/well were counted under a light microscope.

4.7. Animal Experiments

Four-week-old male KK-A^y mice were purchased from CLEA Japan, Inc. (Tokyo, Japan). Mice were housed in individual cages, under a 12-h light/dark cycle and 22 ± 1 °C and were given free access to distilled water. Mice were divided into five groups and fed with one of the following diets for 16 weeks: control diet (a modified AIN-93G containing 10% (*w*/*w*) fat) (*n* = 11), control diet containing 0.005% (*w*/*w*) GW9662 (*n* = 10), 1.0% (*w*/*w*) YMO (*n* = 10), 3.5% (*w*/*w*) YMO (*n* = 10), or 7.0% (*w*/*w*) YMO (*n* = 10). The energy intake of each mice was adjusted by pair feeding.

After 16 weeks of respective dietary treatment, all mice were killed under anesthesia after 16 h of fasting, and blood, each tissue, and femur were collected. All animal experiments were carried out in accordance with the Ethical Guidelines for the Care and Use of Laboratory Animals, Chiba University. The present study was approved by the Ethics Committee for Animal Experiments of Chiba University (Approval No. 30-387).

4.8. OGTT

After 15 weeks of feeding, KK-A^y mice were fasted for 16 h and administered with glucose at 1.5 g/kg body weight by oral gavage. Approximately 40 μL of blood samples were collected from the tail vein at 0, 15, 30, 60, 120 min after glucose administration. Plasma glucose and insulin concentration were measured using Glucose CII-test Wako (FUJIFILM Wako) and Morinaga Ultra-Sensitive Mouse Insulin ELISA Kit (Morinaga Institute of Biological Science, Yokohama, Japan), respectively, according to each manufacturer's protocol. As the index for estimating insulin resistance, homeostasis model assessment-insulin resistance (HOMA-IR) and quantitative insulin-sensitivity check index (QUICKI) were calculated from fasting plasma glucose and insulin concentrations as follows: HOMA-IR = (plasma glucose (mmol/L) at 0 min) × (plasma insulin (μU/mL) at 0 min)/22.5 [49], QUICKI = 1/(log (plasma insulin (μU/mL) at 0 min) + log (plasma glucose (mg/dL) at 0 min)) [50].

4.9. Quantitative Real-Time PCR Analysis

Total RNA was extracted from C3H10T1/2 cells after 14 days of culture and perirenal adipose tissue of KK-A^y mice using RNAiso Plus (Takara Bio inc., Shiga, Japan) according to the manufacturer's protocol. cDNA was synthesized with ReverTra Ace® qPCR RT Master Mix with gDNA Remover (TOYOBO CO., LTD., Osaka, Japan) according to the manufacturer's protocol. Quantitative real-time PCR analysis was performed with Applied Biosystems® StepOnePlus real-time PCR system (Thermo Fisher Scientific, Waltham, MT,

USA) using THUNDERBIRD® SYBR® qPCR Mix (TOYOBO). The PCR amplification was performed as described previously [15]. The primer sequences are listed in Table 3. The expression level of *36B4* mRNA was used as the internal standard for the determination of each target mRNA expression levels.

4.10. Histological Analysis of Adipose Tissues

Perirenal adipose tissues were fixed with 10% formalin for overnight and stored in PBS at 4 °C. Each perirenal adipose tissue was embedded in paraffin and sliced at 0.5 μm using Leica SR 2000 Microtome (Leica Biosystems Nussloch GmbH, Wetzlar, Germany). For hematoxylin and eosin (HE) staining, deparaffinized sections were incubated with Mayer's Hematoxylin Solution (FUJIFILM Wako) for 2 min and 0.25% Eosin Y (FUJIFILM Wako) for 5 min. For immunochemical staining, deparaffinized sections were blocked with 10% Normal Serum Block (SIG-31172, BioLegend, Inc., San Diego, CA, USA) and 2% BSA (Sigma-Aldrich Co.) solution and were incubated with an anti-mouse F4/80 (F4/80 antibody, Cl:A3-1, Bio-Rad Laboratories, Inc., Hercules, CA, USA) (1:200), anti-mouse CD11c (Anti CD11c/Integrin α X, 17342-1-AP, Proteintech Group, Inc., Rosemont, IL, USA) (1:500), or anti-CD206 (Anti-Mannose Receptor antibody, ab64693, Abcam, Cambridge, UK) (1:5000) as the primary antibody at 4 °C overnight. Antigen signals were detected by incubation with biotinylated anti-IgG antibody (Rabbit Anti-Rat IgG Antibody, BA-4001, Vector Laboratories, Burlingame, CA, USA, or Biotin-Conjugated Goat Anti-Rabbit IgG Secondary Antibody, bs-0295G-Biotin, Bioss Antibodies Inc., Woburn, MT, USA), followed by streptavidin-horseradish peroxidase (Abcam) and then DAB (Dojindo Molecular Technologies, Inc., Kumamoto, Japan). Each stained slide was observed under light microscopy and analyzed by Win-ROOF ver. 7.2 (MITANI Corporation, Tokyo, Japan).

4.11. Analysis of Bone Mineral Density (BMD)

The femur of each mouse was used for the analysis of BMD by peripheral quantitative computed tomography (pQCT: LaTheta LCT-100, ALOKA, Tokyo, Japan). BMD was calculated from the bone mineral content of the measured area.

4.12. Measurement of Plasma Bone Metabolic Markers

Plasma ALP activity, a marker of osteoblastic bone formation, and TRAP activity, a marker of osteoclastic bone resorption was measured by Labo assay™ ALP (FUJIFILM Wako) and TRACP & ALP Assay Kit (Takara Bio inc.), respectively, according to each manufacturer's protocol.

4.13. Statistical Analysis

Data are presented as mean ± standard error (SE). Statistical analysis was performed using Bell Curve Excel-Toukei (Social Survey Research Information Co., Tokyo, Japan). The normalization of data was evaluated by Shapiro–Wilk test. Reporter assay data were analyzed by Student's t-test. The other data were analyzed using one-way analysis of value (ANOVA) followed by Dunnett's test or Steel's test. Differences were considered significant at $p < 0.05$.

Table 3. Primers for real-time PCR.

Genes	**Accession Number**	**Forward (5′→3′)**	**Reverse (5′→3′)**
PPARγ	NM_001127330	GGAGATCTCCAGTGATATCGACCA	ACGGCTTCTACGGATCGAAACT
aP2	NM_001122948	AAGACAGCTCCTCCTCGAAGGTT	TGACCAAATCCCCATTTACGC
LPL	NM_008509	GCCCAGCAACATTATCCAGT	GGTCAGACTTCCTGCTACGC
Runx2	DQ065175	CCCAGCCACTTTACCTACA	TATGGAGTGCTGCTGGTCTG
Osterix	AF184902	ACTCATCCCTAATGGCTCGTG	GGTAGGGAGCTGGGTTAAGG
ALP	BC065175	GCTGATCATTCCCACGTTTT	CTGGGCCTGGTAGTTGTTGT
Col1	NM_007742.4	GAGCGGAGAGTACTGGATCG	GCTTCTTTTCCTTGGGGTTC
F4/80	X93328.1	TTTCCTCGCCTGCTTCTTC	CCCCGTCTCTGTATTCAACC
MCP-1	NM_011333.3	AGGTCCCTGTCATGCTTCTG	TCTGGACCCATTCCTTCTTG
CD11c	NM_007482	TGGGTTTGTTTCTTGTCTTG	GCCTGTGTGATAGCCACATTT
IL-1β	NM_008361.4	GCCCATCCTCTGTGACTCAT	AGGCCACAGGTATTTTGTCG
TNF-α	NM_013693	ACACTCAGATCATCTTCTCAAAATTCG	GTGTGGGTGAGGAGCACGTAGT
CD206	NM_008625	GCGCTGCGTGGACGCTCTAA	ACAGGGTGACGGAAGCCCAGT
Ym1	NM_009892	AGAAGGGAGTTTCAAACCTGGT	GTCTTGCTCATGTGTGTAAGTGA
Arg1	NM_007482	CAGTTGGAAGCATCTCTGGC	GTGAGCATCCACCCAAATGAC
36B4	NM_007475.5	TGTGTGTCTGCAGARCGGGTAC	CTTTGGCGGGATTAGTCGAAG

5. Conclusions

We demonstrated that YMO, rich in erucic acid, improved adipose tissue inflammation and insulin resistance. It was also revealed that YMO contributes to the increase of BMD in diabetic mice through the enhancement of bone formation. These results suggest that YMO may contribute to the improvement of impaired glucose and bone metabolism associated with obesity and diabetes.

Supplementary Materials: The following are available online. Table S1: Composition of fatty acids in hydrolyzed YMO, Figure S1: Effect of YMO on adipocytes size and number in perirenal adipose tissue in KK-A^y mice, Figure S2: Effect of YMO on bone mineral density (BMD) in KK-A^y mice.

Author Contributions: Conceptualization, S.H.; investigation, A.T., M.I., and Y.K.; supervision, Y.E. and S.H.; validation, A.T.; writing—original draft, A.T.; writing—review & editing, Y.K., Y.E., and S.H. All authors have read and agreed to the published version of the manuscript.

Funding: This study was funded by Kewpie Corporation.

Institutional Review Board Statement: Animal experiments were carried out in accordance with the Ethical Guidelines for the Care and Use of Laboratory Animals, Chiba University, and approved by the Ethics Committee for Animal Experiments of Chiba University (Approval No. 30-387).

Informed Consent Statement: Not applicable.

Data Availability Statement: Data is contained within the article or Supplementary Material.

Acknowledgments: We gratefully appreciate Kewpie Corporation for providing YMO sample and performing fatty acid analysis. We also appreciate Teruo Kawada and Tsuyoshi Goto, Kyoto University, for providing the vectors used in reporter assay.

Conflicts of Interest: Kewpie Corporation provided research funding and YMO sample. Kewpie Corporation also contributed to the fatty acid analysis. The funder had no role in the design of study, other analysis, interpretation of data, and writing of the manuscript.

Sample Availability: Samples of the compounds are not available from the authors.

References

1. Astrup, A.; Finer, N. Redefining Type 2 Diabetes: 'Diabesity' or 'Obesity Dependent Diabetes Mellitus'? *Obes. Rev.* **2000**, *1*, 57–59. [CrossRef] [PubMed]
2. Salans, L.B.; Cushman, S.W.; Weismann, R.E. Studies of human adipose tissue, Adipose cell size and number in nonobese and obese patients. *J. Clin. Invest.* **1973**, *52*, 929–941. [CrossRef] [PubMed]
3. Siersbaek, R.; Nielsen, R.; Mandrup, S. PPARγ in adipocyte differentiation and metabolism–novel insights from genome-wide studies. *FEBS Lett.* **2010**, *584*, 3242–3249. [CrossRef] [PubMed]
4. Picard, F.; Auwerx, J. PPARγ and glucose homeostasis. *Annu. Rev. Nutr.* **2002**, *22*, 167–197. [CrossRef] [PubMed]
5. Carmona, M.C.; Louche, K.; Nibbelink, M.; Prunet, B.; Bross, A.; Desbazeille, M.; Dacquet, C.; Renard, P.; Casteilla, L.; Pénicaud, L. Fenofibrate prevents Rosiglitazone-induced body weight gain in ob/ob mice. *Int. J. Obes. (Lond.)* **2005**, *29*, 864–871. [CrossRef] [PubMed]
6. Ali, A.A.; Weinstein, R.S.; Stewart, S.A.; Parfitt, A.M.; Manolagas, S.C.; Jilka, R.L. Rosiglitazone causes bone loss in mice by suppressing osteoblast differentiation and bone formation. *Endocrinology* **2005**, *146*, 226–235. [CrossRef]
7. Sottile, V.; Seuwen, K.; Kneissel, M. Enhanced marrow adipogenesis and bone resorption in estrogen-deprived rats treated with the PPARgamma agonist BRL49653 (rosiglitazone). *Calcif. Tissue Int.* **2005**, *75*, 329–337. [CrossRef]
8. Jones, J.R.; Barrick, C.; Kim, K.A.; Lindner, J.; Blondeau, B.; Fujimoto, Y.; Shiota, M.; Kesterson, R.A.; Kahn, B.B.; Magnuson, M.A. Deletion of PPARγ in adipose tissues of mice protects against high fat diet-induced obesity and insulin resistance. *Proc. Natl. Acad. Sci. USA* **2005**, *102*, 6207–6212. [CrossRef]
9. Gumbilai, V.; Ebihara, K.; Aizawa-Abe, M.; Ebihara, C.; Zhao, M.; Yamamoto, Y.; Mashimo, T.; Hosoda, K.; Serikawa, T.; Nakao, K. Fat Mass Reduction With Adipocyte Hypertrophy and Insulin Resistance in Heterozygous PPARγ Mutant Rats. *Diabetes* **2016**, *65*, 2954–2965. [CrossRef]
10. Yamauchi, T.; Kamon, J.; Waki, H.; Murakami, K.; Motojima, K.; Komeda, K.; Ide, T.; Kubota, N.; Terauchi, Y.; Tobe, K.; et al. The mechanisms by which both heterozygous peroxisome proliferator-activated receptor γ (PPARγ) deficiency and PPARγ agonist improve insulin resistance. *J. Biol. Chem.* **2001**, *276*, 41245–41254. [CrossRef]
11. Nakano, R.; Kurosaki, E.; Yoshida, S.; Yokono, M.; Shimaya, A.; Maruyama, T.; Shibasaki, M. Antagonism of peroxisome proliferator-activated receptor γ prevents high-fat diet-induced obesity in vivo. *Biochem. Pharmacol.* **2006**, *72*, 42–52. [CrossRef] [PubMed]

12. Yamauchi, T.; Waki, H.; Kamon, J.; Murakami, K.; Motojima, K.; Komeda, K.; Miki, H.; Kubota, N.; Terauchi, Y.; Tsuchida, A.; et al. Inhibition of RXR and PPARγ ameliorates diet-induced obesity and type 2 diabetes. *J. Clin. Investig.* **2001**, *108*, 1001–1013. [CrossRef] [PubMed]
13. Duque, G.; Li, W.; Vidal, C.; Bermeo, S.; Rivas, D.; Henderson, J. Pharmacological inhibition of PPARγ increases osteoblastogenesis and bone mass in male C57BL/6 mice. *J. Bone Miner. Res.* **2013**, *28*, 639–648. [CrossRef]
14. David, V.; Martin, A.; Lafage-Proust, M.H.; Malaval, L.; Peyroche, S.; Jones, D.B.; Vico, L.; Guignandon, A. Mechanical loading down-regulates peroxisome proliferator-activated receptor γ in bone marrow stromal cells and favors osteoblastogenesis at the expense of adipogenesis. *Endocrinology* **2007**, *148*, 2553–2562. [CrossRef] [PubMed]
15. Takahashi, A.; Dohi, H.; Egashira, Y.; Hirai, S. Erucic acid derived from rosemary regulates differentiation of mesenchymal stem cells into osteoblasts/adipocytes via suppression of peroxisome proliferator-activated receptor γ transcriptional activity. *Phytother. Res.* **2020**, *34*, 1358–1366. [CrossRef]
16. Ishaq, M.; Razi, R.; Khan, S.A. Exploring genotypic variations for improved oil content and healthy fatty acids composition in rapeseed (Brassica napus L.). *J. Sci. Food Agric.* **2017**, *97*, 1924–1930. [CrossRef]
17. Wendlinger, C.; Hammann, S.; Vetter, W. Various concentrations of erucic acid in mustard oil and mustard. *Food Chem.* **2014**, *153*, 393–397. [CrossRef]
18. Ciubota-Rosie, C.; Macoveanu, M.; Fernàndez, C.M.; Ramos, M.J.; Pérez, A.; Moreno, A. Sinapis alba seed as a prospective biodiesel source. *Biomass Bioenergy* **2013**, *53*, 83–90. [CrossRef]
19. Tzen, J.; Cao, Y.; Laurent, P.; Ratnayake, C.; Huang, A. Lipids, Proteins, and Structure of Seed Oil Bodies from Diverse Species. *Plant Physiol.* **1993**, *101*, 267–276. [CrossRef]
20. Ducy, P.; Starbuck, M.; Priemel, M.; Shen, J.; Pinero, G.; Geoffroy, V.; Amling, M.; Karsenty, G.A. Cbfa1-dependent genetic pathway controls bone formation beyond embryonic development. *Genes Dev.* **1999**, *13*, 1025–1036. [CrossRef]
21. Nakashima, K.; Zhou, X.; Kunkel, G.; Zhang, Z.; Deng, J.M.; Behringer, R.R.; de Crombrugghe, B. The novel zinc finger-containing transcription factor osterix is required for osteoblast differentiation and bone formation. *Cell* **2002**, *108*, 17–29. [CrossRef]
22. Xu, F.; Dong, Y.; Huang, X.; Li, M.; Qin, L.; Ren, Y.; Guo, F.; Chen, A.; Huang, S. Decreased osteoclastogenesis, osteoblastogenesis and low bone mass in a mouse model of type 2 diabetes. *Mol. Med. Rep.* **2014**, *10*, 1935–1941. [CrossRef] [PubMed]
23. Takasawa, K.; Kubota, N.; Terauchi, Y.; Kadowaki, T. Impact of increased PPARγ activity in adipocytes in vivo on adiposity, insulin sensitivity and the effects of rosiglitazone treatment. *Endocr. J.* **2008**, *55*, 767–776. [CrossRef] [PubMed]
24. Okuno, A.; Tamemoto, H.; Tobe, K.; Ueki, K.; Mori, Y.; Iwamoto, K.; Umesono, K.; Akanuma, Y.; Fujiwara, T.; Horikoshi, H.; et al. Troglitazone increases the number of small adipocytes without the change of white adipose tissue mass in obese Zucker rats. *J. Clin. Investig.* **1998**, *101*, 1354–1361. [CrossRef] [PubMed]
25. Ding, L.; Jin, D.; Chen, X. Luteolin enhances insulin sensitivity via activation of PPARγ transcriptional activity in adipocytes. *J. Nutr. Biochem.* **2010**, *21*, 941–947. [CrossRef]
26. Takahashi, N.; Goto, T.; Taimatsu, A.; Egawa, K.; Katoh, S.; Kusudo, T.; Sakamoto, T.; Ohyane, C.; Lee, J.Y.; Kim, Y.I.; et al. Bixin regulates mRNA expression involved in adipogenesis and enhances insulin sensitivity in 3T3-L1 adipocytes through PPARγ activation. *Biochem. Biophys. Res. Commun.* **2009**, *390*, 1372–1376. [CrossRef]
27. Kennedy, A.; Chung, S.; LaPoint, K.; Fabiyi, O.; McIntosh, M.K. Trans-10, cis-12 conjugated linoleic acid antagonizes ligand-dependent PPARγ activity in primary cultures of human adipocytes. *J. Nutr.* **2008**, *138*, 455–461. [CrossRef]
28. Platt, I.D.; El-Sohemy, A. Regulation of osteoblast and adipocyte differentiation from human mesenchymal stem cells by conjugated linoleic acid. *J. Nutr. Biochem.* **2009**, *20*, 956–964. [CrossRef]
29. Smith, R.H.; Powell, G.L. The critical micelle concentration of some physiologically important fatty acyl-coenzyme A's as a function of chain length. *Arch. Biochem. Biophys.* **1986**, *244*, 357–360. [CrossRef]
30. Kassem, M.; Philippe, F.; Isabelle, W. Adipose tissue in obesity-related inflammation and insulin resistance: Cells, cytokines, and chemokines. *ISRN Inflamm.* **2013**. [CrossRef]
31. Yu, R.; Kim, C.S.; Kwon, B.S.; Kawada, T. Mesenteric Adipose Tissue-Derived Monocyte Chemoattractant Protein-1 Plays a Crucial Role in Adipose Tissue Macrophage Migration and Activation in Obese Mice. *Obesity* **2006**, *14*, 1353–1362. [CrossRef] [PubMed]
32. Kamei, N.; Tobe, K.; Suzuki, R.; Ohsugi, M.; Watanabe, T.; Kubota, N.; Ohtsuka-Kowatari, N.; Kumagai, K.; Sakamoto, K.; Kobayashi, M.; et al. Overexpression of monocyte chemoattractant protein-1 in adipose tissues causes macrophage recruitment and insulin resistance. *J. Biol. Chem.* **2006**, *281*, 26602–26614. [CrossRef] [PubMed]
33. Fujisaka, S.; Usui, I.; Bukhari, A.; Ikutani, M.; Oya, T.; Kanatani, Y.; Tsuneyama, K.; Nagai, Y.; Takatsu, K.; Urakaze, M.; et al. Regulatory mechanisms for adipose tissue M1 and M2 macrophages in diet-induced obese mice. *Diabetes* **2009**, *58*, 2574–2582. [CrossRef] [PubMed]
34. Hill, A.A.; Reid Bolus, W.; Hasty, A.H. A decade of progress in adipose tissue macrophage biology. *Immunol. Rev.* **2014**, *262*, 134–152. [CrossRef]
35. Cinti, S.; Mitchell, G.; Barbatelli, G.; Murano, I.; Ceresi, E.; Faloia, E.; Wang, S.; Fortier, M.; Greenberg, A.S.; Obin, M.S. Adipocyte death defines macrophage localization and function in adipose tissue of obese mice and humans. *J. Lipid Res.* **2005**, *46*, 2347–2355. [CrossRef]
36. Choi, J.H.; Banks, A.S.; Estall, J.L.; Kajimura, S.; Boström, P.; Laznik, D.; Ruas, J.L.; Chalmers, M.J.; Kamenecka, T.M.; Blüher, M.; et al. Anti-diabetic drugs inhibit obesity-linked phosphorylation of PPARgamma by Cdk5. *Nature* **2010**, *466*, 451–456. [CrossRef]

37. Choi, J.H.; Banks, A.S.; Kamenecka, T.M.; Busby, S.A.; Chalmers, M.J.; Kumar, N.; Kuruvilla, D.S.; Shin, Y.; He, Y.; Bruning, J.B.; et al. Antidiabetic actions of a non-agonist PPARγ ligand blocking Cdk5-mediated phosphorylation. *Nature* **2011**, *477*, 477–481. [CrossRef]
38. Banks, A.S.; McAllister, F.E.; Camporez, J.P.; Zushin, P.J.; Jurczak, M.J.; Laznik-Bogoslavski, D.; Shulman, G.I.; Gygi, S.P.; Spiegelman, B.M. An ERK/Cdk5 axis controls the diabetogenic actions of PPARγ. *Nature* **2015**, *517*, 391–395. [CrossRef]
39. Lu, Y.; Zhou, Q.; Zhong, F.; Guo, S.; Hao, X.; Li, C.; Wang, W.; Chen, N. 15-Deoxy-$\Delta^{12,14}$-Prostaglandin J2 Modulates Lipopolysaccharide-Induced Chemokine Expression by Blocking Nuclear Factor-κB Activation via Peroxisome Proliferator Activated Receptor-γ-Independent Mechanism in Renal Tubular Epithelial Cells. *Nephron. Exp. Nephrol.* **2013**, *123*, 1–10. [CrossRef]
40. Choi, S.S.; Kim, E.S.; Jung, J.E.; Marciano, D.P.; Jo, A.; Koo, J.Y.; Choi, S.Y.; Yang, Y.R.; Jang, H.J.; Kim, E.K.; et al. PPARγ Antagonist Gleevec Improves Insulin Sensitivity and Promotes the Browning of White Adipose Tissue. *Diabetes* **2016**, *65*, 829–839. [CrossRef]
41. Shui, C.; Spelsberg, T.C.; Riggs, B.L.; Khosla, S. Changes in Runx2/Cbfa1 expression and activity during osteoblastic differentiation of human bone marrow stromal cells. *J. Bone Miner. Res.* **2003**, *18*, 213–221. [CrossRef] [PubMed]
42. Hinoi, E.; Fujimori, S.; Wang, L.; Hojo, H.; Uno, K.; Yoneda, Y. Nrf2 negatively regulates osteoblast differentiation via interfering with Runx2-dependent transcriptional activation. *J. Biol. Chem.* **2006**, *281*, 18015–18024. [CrossRef] [PubMed]
43. Léotoing, L.; Davicco, M.J.; Lebecque, P.; Wittrant, Y.; Coxam, V. The flavonoid fisetin promotes osteoblasts differentiation through Runx2 transcriptional activity. *Mol. Nutr. Food Res.* **2014**, *58*, 1239–1248. [CrossRef] [PubMed]
44. Kim, Y.J.; Lee, M.H.; Wozney, J.M.; Cho, J.Y.; Ryoo, H.M. Bone morphogenetic protein-2-induced alkaline phosphatase expression is stimulated by Dlx5 and repressed by Msx2. *J. Biol. Chem.* **2004**, *279*, 50773–50780. [CrossRef]
45. Felthaus, O.; Gosau, M.; Klein, S.; Prantl, L.; Reichert, T.E.; Schmalz, G.; Morsczeck, C. Dexamethasone-related osteogenic differentiation of dental follicle cells depends on ZBTB16 but not Runx2. *Cell Tissue Res.* **2014**, *357*, 695–705. [CrossRef]
46. Beekman, K.M.; Veldhuis-Vlug, A.G.; van der Veen, A.; den Heijer, M.; Maas, M.; Kerckhofs, G.; Parac-Vogt, T.N.; Bisschop, P.H.; Bravenboer, N. The effect of PPARγ inhibition on bone marrow adipose tissue and bone in C3H/HeJ mice. *Am. J. Physiol. Endocrinol. Metab.* **2019**, *316*, E96–E105. [CrossRef]
47. Wronski, T.J.; Cintrón, M.; Dann, L.M. Temporal relationship between bone loss and increased bone turnover in ovariectomized rats. *Calcif. Tissue Int.* **1988**, *43*, 179–183. [CrossRef]
48. Leslie, W.D.; Rubin, M.R.; Schwartz, A.V.; Kanis, J.A. Type 2 diabetes and bone. *J. Bone Miner. Res.* **2012**, *27*, 2231–2237. [CrossRef]
49. Wallace, T.M.; Levy, J.C.; Matthews, D.R. Use and abuse of HOMA modeling. *Diabetes Care* **2004**, *27*, 1487–1495. [CrossRef]
50. Muniyappa, R.; Lee, S.; Chen, H.; Quon, M.J. Current approaches for assessing insulin sensitivity and resistance in vivo: Advantages, limitations, and appropriate usage. *Am. J. Physiol. Endocrinol. Metab.* **2008**, *294*, E15–E26. [CrossRef]